Proceedings of the ASME 2012 International Mechanical Engineering Congress & Exposition
IMECE2012
November 9-15, 2012, Houston, Texas, USA

IMECE2012-85555

UNCERTAINTY ANALYSIS OF SOLID-LIQUID-VAPOR PHASE CHANGE OF A METAL PARTICLE SUBJECT TO NANOSECOND LASER HEATING

Hao Peng, Yuwen Zhang, and P. Frank Pai
Department of Mechanical and Aerospace Engineering
University of Missouri
Columbia MO 65211, USA
Email: zhangyu@missouri.edu

ABSTRACT

Effects of uncertainties of various parameters, including laser fluence, diameter of metal powder articles, laser pulse width and initial temperature of metal particles, on solid-liquid-vapor phase change processes of metal particles under nanosecond laser heating are investigated in this paper. A systematic approach of simulating phase change with uncertain parameters are presented and a sample-based stochastic model are established to investigate the influence of different uncertain parameters on maximum surface temperature of metal particles, maximum solid-liquid interface location, maximum liquid-vapor interface location, maximum saturation temperature and maximum recoil pressure, and time needed to reach maximum solid-liquid interface location. The results show that the mean value and standard deviation of laser fluence have dominant effects on all output parameters.

INTRODUCTION

In selective laser sintering (SLS) process, fine parts can be obtained by fusing micro- or nano-sized metal particles with nanosecond lasers [1-7]. When the metal particle is heated by the laser pulse, the temperature of the metal article increases rapidly; followed by partial melting of the metal particle from the surface. The liquid metal engages the space between metal articles which is originally occupied by air. As the temperature of the liquid phase metal gets higher, evaporation occurs and metal particle will be surrounded by metal gas at saturation temperature [8]. When the laser pulse of off, the temperature of liquid metal decreases and liquid metal resolidifies. If laser beam scans through the metal particle bed, the melting and resolidification processes will repeat again and again and a layer of the part can be created.

Although modeling of SLS has advanced significantly in the recent years, effects of the inherent uncertainty of processing parameters that can directly cause unstable characteristics of products are not fully understood. The fluence and width of laser pulse of the nanosecond laser may fluctuate. In addition, the sizes of metal powder particles in the powder bed cannot be mono-sized but rather have certain size distribution. The initial metal powder temperature also differs largely due to fluctuation of ambient temperature and heating by previous laser pulses. These parametric uncertainties will possibly render characteristics in phase change processes, which, in turn, causes uncertainties of metal powder surface temperature, positions of solid-liquid and liquid-vapor interfaces, saturation temperature and recoil pressure, and time at which solid-liquid interface reaches maximum. Therefore, analysis of parametric uncertainty is imperative in a realistic, physical-based simulation of phase change of metal particles under nanosecond laser heating. Acquah et al. presented an approach to analyze uncertainty by posing and solving two-stage optimization problem (TSOP) [9]. One disadvantage of this method was that parameter uncertainty distribution cannot be included.

In order to incorporate parametric uncertainty distribution, a systematic methodology, which is called sample-based stochastic model, was proposed to analyze effects of uncertainty of parameters. Padmanabhan et al. applied the stochastic model to investigate the effect of uncertainty in process and material on the nonisothermal filling process [10]. Diwekar et al. improved the conventional simulation models and process simulators with the stochastic modeling implemented in the ASPEN process simulator [11]. Effects of uncertainty in optical fiber drawing process on the variability of index of refraction, residual stress, maximum tension, and defection concentration were also investigated with a sampling-based stochastic model [12-13]. More applications of stochastic model can be found in thermosetting-matrix composites fabrication, proton exchange membrane (PEM) fuel cells,

sheetpile cofferdam design and safety assessments of technological systems [14-17].

In this paper, the sample-based stochastic model will be applied to study the phase change processes of metal particle under uncertain laser fluence, metal particle size, pulse width, and initial temperature to reveal different influence of these parameters. Figure 1 is depicted to elucidate how the stochastic method is applied in the analysis of metal powder phase change processes. Analysis conducted in this paper can provide important information in controlling these parameters in research or manufacturing process.

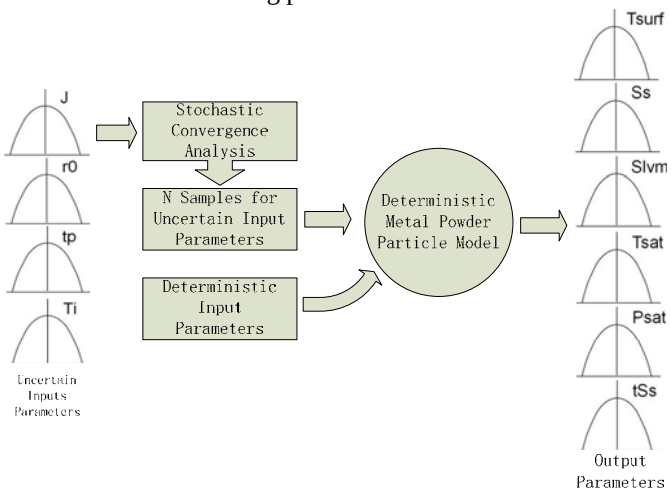

Fig. 1 Sample-Based Stochastic Model

NOMENCLATURE

h_{sl}	latent heat of fusion, $J \cdot kg^{-1}$
h_{lv}	latent heat of vaporization, $J \cdot kg^{-1}$
k	thermal conductivity, $W \cdot m^{-1} \cdot K^{-1}$
p_0	atmospheric pressure, Pa
q''	heat flux, $W \cdot m^{-2}$
q_0''	maximum heat flux, $W \cdot m^{-2}$
R_g	gas constant, $J \cdot kg^{-1} \cdot K^{-1}$
r_0	radius of metal particle, m
S_s	solid-liquid interface location, m
S_l	liquid-vapor interface location, m
T	temperature, K
$T_{sat,0}$	saturation temperature at atmospheric pressure, K
t	time, s
t_m	time when melting begins, s
t_p	half width of the laser beam pulse at $q_0''/2$, s
t_r	time when melting and resolidification begins, s
t_s	time when solidification ends, s
t_v	time when vaporization begins, s
x	distance measured from the surface of the particle, m

Greek Symbols

α	thermal diffusivity, $m^2 \cdot s^{-1}$
δ	penetration depth, m
γ	specific heat ratio
θ	$T - T_i$, excess temperature
ρ	density, $kg \cdot m^{-3}$
τ	t / t_p, relative time with t_p
μ	mean value
σ	standard deviation

Subscripts

i	initial
l	liquid
m	melting
r	resolidification
s	solid or solidification
sat	saturation
v	vapor or vaporization

PHYSICAL MODEL

Phase change of a single metal powder particle under nanosecond laser heating will be investigated. When the laser beam scans across the powder bed, it can penetrate into the powder bed and reflection takes place at the surface of metal particles. With consideration of these facts, homogeneous heating flux around metal particles is assumed. Because of spherical symmetric geometry of metal powder particle, the model can be further simplified to a 1-D problem, as shown in Fig. 2. Temporal Gaussian heat flux [18-19] is assumed for laser and the origin of time is chosen to be the time when heat flux is at maximum. Thus the heat flux with respect to time is

$$q"(t) = q_0'' e^{-ln2\frac{t^2}{t_p^2}} \quad (1)$$

where q_0'' is the maximum heat flux and t_p is the pulse width (see Fig. 2).

The fluence of laser that reaches the metal powder particle surface $J(W/m^2)$ can be related to the integration of laser heat flux with respect to time

$$J = \int_{-\infty}^{\infty} q"(t)dt = \int_{-\infty}^{\infty} q_0'' e^{-ln2\frac{t^2}{t_p^2}} dt = 2q_0'' t_p \frac{\sqrt{\pi}}{\sqrt{ln\,2}} \quad (2)$$

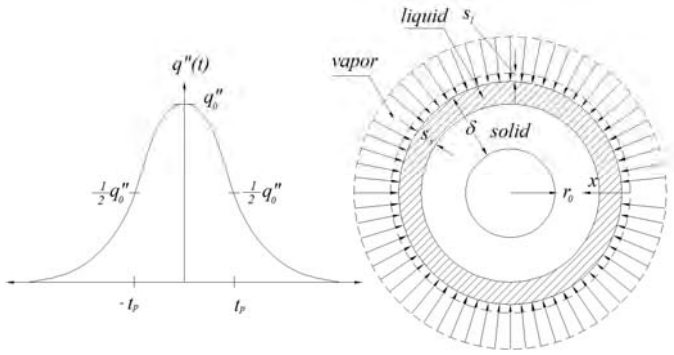

Fig. 2 Physical Model

The phase change process consists of following stages: preheating, melting and vaporization, melting, resolidification and thermalization. Some assumptions must be made to establish the physical model: (1) although thermal conductivity and thermal diffusivity of metal particles will be affected by

metal phase change, they are assumed to be temperature independent. (2) Heat transfer from the liquid surface to the outside is neglected. (3) Evaporated metal will not condensate back to the metal powder particle. (4) Heat flux received by metal particles is kept constant regardless of metal particle phase change or temperature fluctuation as well as variation of particles sizes.

Governing Equations

Preheating Stage ($t<t_m$)

In the preheating stage, heat is transferred from metal powder particle surface to the interior by conduction. The heat conduction equation in the particle is

$$\frac{\alpha_s}{(r_0-x)^2}\frac{\partial}{\partial x}\left((r_0-x)^2\frac{\partial \theta_s}{\partial x}\right)=\frac{\partial \theta_s}{\partial t} \quad (3)$$

where $\theta_s = T_s - T_i$ is excess temperature. The initial and boundary conditions for Eq. (3) are

$$\theta_s = 0, 0 \le x \le r_0, t \to -\infty \quad (4)$$

$$\frac{\partial \theta_s}{\partial x} = 0, x = r_0 \quad (5)$$

$$-k_s\frac{\partial \theta_s}{\partial x} = q''(t), x = 0 \quad (6)$$

Melting Stage ($t_m < t < t_v$)

The governing equation in the liquid phase ($0 \le x \le S_s(t)$) is

$$\frac{\alpha_l}{(r_0-x)^2}\frac{\partial}{\partial x}\left((r_0-x)^2\frac{\partial \theta_l}{\partial x}\right)=\frac{\partial \theta_l}{\partial t} \quad (7)$$

where $\theta_l = T_l - T_i$. Boundary condition for Eq. (7) is

$$-k_l\frac{\partial \theta_l}{\partial x} = q''(t), \quad x = 0 \quad (8)$$

In the solid phase ($S_s(t) \le x \le r_0$), Eqs. (3) and (5) are still applicable. The boundary conditions at the solid-liquid interface are

$$\theta_s(x,t) = \theta_l(x,t) = T_m - T_i, \ x = S_s(t) \quad (9)$$

$$-k_l\frac{\partial \theta_l}{\partial x} = \frac{dS_s}{dt}h_{sl}\rho_s - k_s\frac{\partial \theta_s}{\partial x}, \ x = S_s(t) \quad (10)$$

The initial temperature distribution at melting stage is the same with the final temperature distribution in the preheating stage.

Vaporization Stage ($t_v < t < t_r$)

Governing equation at liquid phase is still Eq. (7) but the boundary conditions at the liquid surface (liquid-vapor interface) are

$$\theta_l(x,t) = \theta_{sat} = T_{sat} - T_i, \ x = S_l(t) \quad (11)$$

$$\rho_l h_{lv}\frac{dS_l}{dt} - k_l\frac{\partial \theta_l}{\partial x} = q''(t), \ x = S_l(t) \quad (12)$$

Governing equations and boundary conditions at solid phase and solid-liquid interface are still Eqs. (3), (5), (9), and (10). Initial temperature distribution in this stage is the same with the final temperature distribution in the melting stage.

Melting and Resolidification Stage ($t_r < t < t_s$)

Governing equation and boundary conditions in this stage are the same as the melting stage. The point that should be kept in mind is that the radius of metal powder article decreases due to the assumption that evaporated metal will not condense back to the metal powder surface. The initial condition in this stage is the final temperature distribution in the vaporization stage.

Thermalization Stage ($t > t_s$)

Thermalization stage is similar to preheating stage, during which conduction is the only mechanism of heat transfer. The Eqs. (3) and (5) for preheating are still valid in this stage. Taking the fact that laser pulse is so weak that can be omitted into consideration, boundary condition at the metal particle surface can be added

$$\frac{\partial \theta_s}{\partial x} = 0, x = 0, t>t_s \quad (13)$$

INTEGRAL SOLUTIONS

Temperature distribution in different stages can be obtained through an integral approximate method. Before introducing the integral method, a concept of thermal penetration depth should be explained. When heat flux reaches the surface of metal particle, heat will conduct inward. The depth heat can reach at a given time is called thermal penetration depth, noted with δ. At the thermal penetration depth, the following boundary conditions are valid:

$$\theta_s = 0, x \ge \delta(t), t>-\infty \quad (14)$$

$$\frac{\partial \theta_s}{\partial x} = 0, x \ge \delta(t), t>-\infty \quad (15)$$

Preheating and Melting Stages

Integral method can be applied to solve problems in preheating and melting stages [8]. The thermal penetration depth during preheating stage can be obtained from:

$$\frac{1}{60}\delta^4 e^{-\ln 2\frac{t^2}{\tau_p^2}} - \frac{1}{12}\delta^3 r_0 e^{-\ln 2\frac{t^2}{\tau_p^2}} + \frac{1}{6}\delta^2 r_0^2 e^{-\ln 2\frac{t^2}{\tau_p^2}} - \frac{\alpha_s r_0^2 \tau_p\sqrt{\pi}}{2\sqrt{\ln 2}}\left[1 + \operatorname{erf}\left(\sqrt{\ln 2}\frac{t}{\tau_p}\right)\right] = 0 \quad (16)$$

The thermal penetration depth is the only one real positive root of Eq. (16). The temperature distribution in metal particle during the preheating stage is

$$\theta_s(x,t) = \frac{q_0''(\delta-x)^2}{2k_s\delta}e^{-\ln 2\frac{t^2}{\tau_p^2}}, \delta < r_0, t < t_m \quad (17)$$

During the melting stage, the thermal penetration depth δ can be obtain through following equation

$$\delta^3 + \delta^2(-5r_0 + 2S_s) + \delta(10r_0^2 - 10r_0S_s + 3S_s^2) + \left[20r_0^2S_s - 15r_0S_s^2 + 4S_s^3 - 10r_0^2\delta_m + 5r_0\delta_m^2 - \delta_m^3 - 60\alpha_s\int_{t_m}^{t}\frac{(r_0-S_s)^2}{(\delta-S_s)}dt\right] = 0 \quad (18)$$

where δ_m is penetration when melting stage starts. The location of solid liquid interface S_s can be obtained from

$$S_s = \frac{q_0'' r_0^2}{h_{sl}\rho_s}\int_{t_m}^{t}\frac{1}{(r_0-x)^2}e^{-\ln 2\frac{t^2}{\tau_p^2}}dt - \frac{2k_s(T_m-T_l)}{h_{sl}\rho_s}\int_{t_m}^{t}\frac{1}{\delta-S_s}dt \quad (19)$$

The temperature distributions in the solid and liquid phases in this stage are

$$\theta_s(x,t) = \frac{(T_m-T_l)}{(\delta-S_s)^2}(\delta-x)^2, t_m < t < t_s \quad (20)$$

$$\theta_l(x,t) = \frac{q_0'' r_0^2}{k_l}e^{-\ln 2\frac{t^2}{\tau_p^2}}\left(\frac{1}{r_0-S_s} - \frac{1}{r_0-x}\right) + (T_m - T_l), t_m < t < t_s \quad (21)$$

Vaporization Stage

Integrating both sides of Eq. (3) with respect to x from S_s to δ, and considering Eqs. (6), (14), and (15), one gets

$$\frac{\partial}{\partial t}\int_{S_s}^{\delta}\theta_s(r_0-x)^2dx+(T_m-T_l)(r_0-S_s)^2\frac{dS_s}{dt}=-\alpha_s(r_0-S_s)^2\frac{\partial\theta_s}{\partial t}|_{x=S_s} \quad (22)$$

Assuming that temperature distribution in solid phase is a polynomial function and employing Eqs. (9) (15) and (16), temperature in solid phase becomes

$$\theta_s(x,t)=\frac{(T_m-T_l)(x-\delta)^2}{(S_s-\delta)^2} \quad (23)$$

Substituting Eq. (23) into Eq. (22), one obtains

$$\frac{d}{dt}(-10r_0^2S_s+15r_0S_s^2-6S_s^3+10r_0^2\delta-10r_0S_s\delta+3S_s^2\delta-5r_0\delta^2+2S_s\delta^2+\delta^3)+30(r_0-S_s)^2\frac{dSs}{dt}=-60\alpha_s\frac{(r_0-S_s)^2}{(S_s-\delta)} \quad (24)$$

Integrating both sides of Eq. (24) with respect to t from t_v to t, and collecting terms of δ gives

$$\delta^3+\delta^2(-5r_0+2S_s)+\delta(10r_0^2-10r_0S_s+3S_s^2)+\Big[20r_0^2(S_s-S_{sv})-15r_0(S_s^2-S_{sv}^2)+4(S_s^3-S_{sv}^3)-10r_0^2\delta_v+10r_0S_{sv}\delta_v-3S_{sv}^2\delta_v+5r_0\delta_v^2-2S_{sv}\delta_v^2-\delta_v^3-60\alpha_s\int_{l_v}^{l}\frac{(r_0-S_s)^2}{(\delta-S_s)}dt\Big]=0 \quad (25)$$

where S_{sv} and δ_v are S_s and δ when vaporization begins.

Assuming the temperature distribution function is $\theta_l(x,t)=A_l/(r_0-x)+B_l$ and applying Eqs. (9) and (12) to solve A_l and B_l gives

$$\theta_l(x,t)=T_{sat}-T_l+\frac{(T_{sat}-T_m)(r_0-S_s)(x-S_l)}{(r_0-x)(S_l-S_s)} \quad (26)$$

Substituting Eqs. (1) and (26) into Eq. (11) and integrating equation obtained with respect to t from t_v to t yields

$$S_l=\frac{1}{\rho_l h_{lv}}\left[\int_{t_v}^{t}q_0''e^{-\ln 2\frac{t^2}{\tau_p^2}}dt+k_l\int_{t_v}^{t}\frac{(T_{sat}-T_m)(r_0-S_s)}{(r_0-S_l)(S_l-S_s)}dt\right] \quad (27)$$

Substituting Eqs. (23) and (26) into Eq. (10) and integrating the equation obtained with respect to t from t_v to t yields

$$S_s=\frac{1}{\rho_s h_{sl}}\left[2k_s\int_{t_v}^{t}\frac{(T_m-T_0)}{(S_s-\delta)}dt-k_l\int_{t_v}^{t}\frac{(T_{sat}-T_m)(r_0-S_l)}{(r_0-S_s)(S_l-S_s)}dt\right]+S_{sv} \quad (28)$$

where S_{sv} is the value of S_s when vaporization begins.

In vaporization stage, metal vapor surrounds the metal particle surface, which creates recoil pressure and increases saturation temperature for vaporization. Through the Clausius /Clapeyron equation and a gas dynamic model [20, 21], one can obtains the relation between saturation temperature and surface heat flux.

$$\frac{\gamma+1}{\gamma h_{lv}}\sqrt{\gamma R_g T_{sat}}\left(q''+k_l\frac{\partial\theta_l}{\partial x}\right)=p_0\exp\left[\frac{h_{lv}}{R_g}\left(\frac{1}{T_{sat,0}}-\frac{1}{T_{sat}}\right)\right] \quad (29)$$

where p_0 is atmospheric pressure and $T_{sat,0}$ is saturation temperature at this pressure.

Substituting Eqs. (1) and (26), into Eq. (29) gives

$$T_{sat}=\frac{(S_l-S_s)(r_0-S_l)}{k_l(r_0-S_s)}\left\{\frac{\gamma h_{lv}p_0}{(\gamma+1)\sqrt{\gamma R_g T_{sat}}}\exp\left[\frac{h_{lv}}{R_g}\left(\frac{1}{T_{sat,0}}-\frac{1}{T_{sat}}\right)\right]-q_0''e^{-\ln 2\frac{t^2}{\tau_p^2}}\right\}+T_m \quad (30)$$

The vaporization stage is described by four nonlinear equations (25), (27), (28) and (30) for four unknowns: δ, S_s, S_l and T_{sat}, which can be solved by an iterative method.

Melting and Resolidification Stage and Thermalization Stage.

Because governing equations for melting and resolidification stage is same with the melting stage, the solution of this stage is also the same as that of the melting stage except reduced radius due to vaporization. Thermalization stage is the same as preheating stage except that initial temperature of this stage is the final temperature of melting and resolidification stage. Integral method applied in preheating stage should be modified before being used in thermalization stage because of non-uniform initial temperature of this stage.

SIMULATION UNDER UNCERTAINTY

Uncertain input parameters investigated here are laser fluence J, metal powder particle radius r_0, laser pulse width t_p, and the initial temperature T_i. Due to the difficulties in obtaining experimental distribution of these uncertain parameters, it is assumed that all these input parameters obey Gaussian distribution [12]. Gaussian distribution is characterized by mean value (μ), which denotes the nominal value of the uncertain parameters, and standard deviation (σ), which represents the uncertainty of the parameters. To represent the degree of uncertainty of input parameters, coefficient of variance (COV), which is defined as σ/μ, is used. COV of certain parameters is zero according to the definition and parameters with high standard deviation and low nominal mean value have high COV.

The first step is to select enough samples for input parameters with uncertainty. To guarantee samples selected from Gaussian distribution are representative, a stochastic convergence analysis is conducted. Standard deviation and mean value of input parameters and output parameters with different number of samples are analyzed. When number of samples increase, the mean value and standard deviation of input parameters converge to the nominal mean value and standard deviation of Gaussian distribution and mean value and standard deviation of output parameters will also converge within certain tolerance [12].

After selecting enough samples, for every input sample, a deterministic physical model discussed in the previous two sections is applied to simulate the solid-liquid-vapor phase change process. Output parameters of interest in this study include: maximum temperature T_{surf} at the metal powder surface; maximum solid-liquid interface S_s; maximum liquid-vapor interface S_{lvm}; maximum saturation temperature T_{sat}; maximum saturation pressure P_{sat}; and time t_{Ss} needed to reach maximum S_s. When input parameters J, r_0, t_p, T_i are

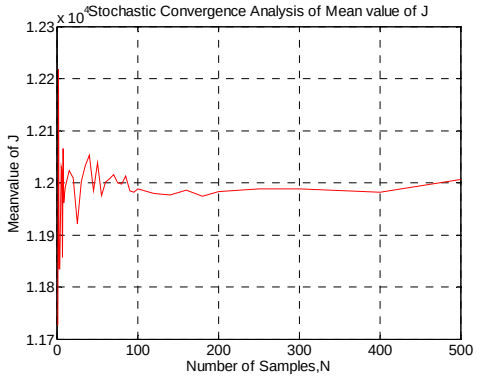

(a) Convergence Analysis of Mean Value of J

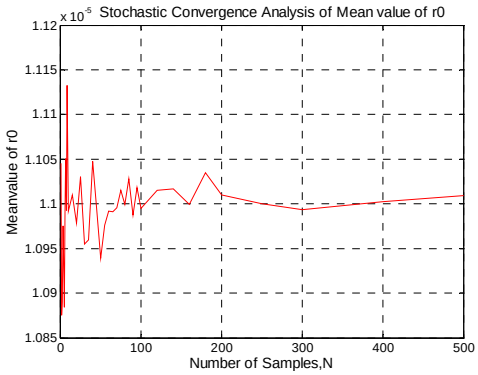

(b) Convergence Analysis of Mean Value of r_0

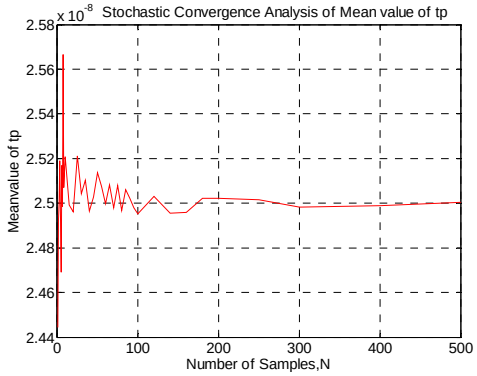

(c) Convergence Analysis of Mean Value of t_p

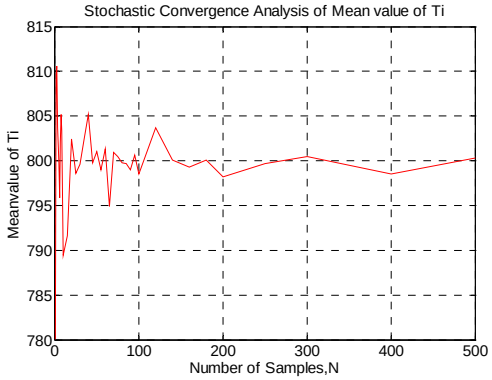

(d) Convergence Analysis of Mean Value of T_i

Fig. 3 Stochastic Convergence Analysis of Input Parameters

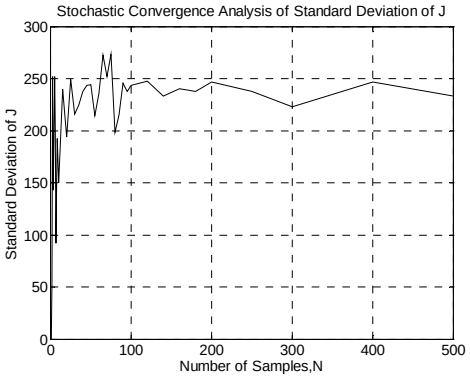

(a)Convergence Analysis of Standard Deviation of J

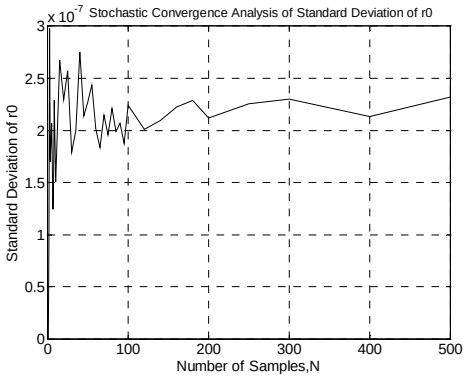

(b)Convergence Analysis of Standard Deviation of r_0

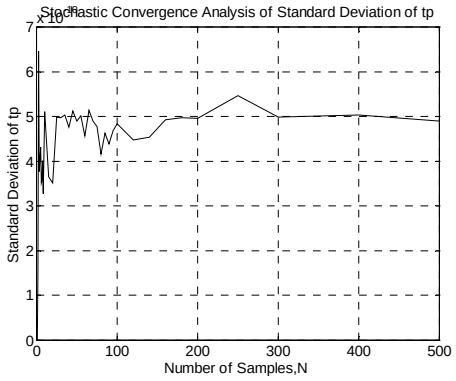

(c)Convergence Analysis of Standard Deviation of t_p

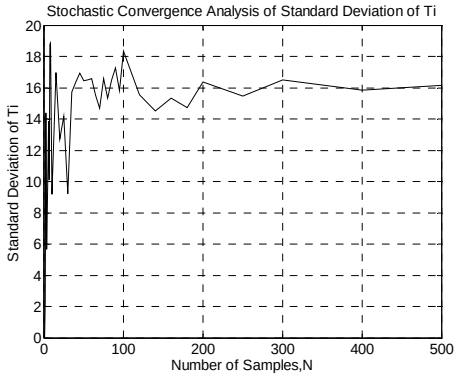

(d)Convergence Analysis of Standard Deviation of T_i

Fig. 4 Stochastic Convergence Analysis of Standard Deviation of Input Parameters

subjected to uncertainty, output parameters T_{surf}, S_s, S_{lvm}, T_{sat}, P_{sat} and t_{Ss} should also be uncertain. To quantify the uncertainty of output parameters, interquartile range (IQR) is defined as the difference between the 25th percentile (P25) and the 75th percentile (P75) [12].

$$IQR = P75 - P25 \quad (18)$$

RESULTS AND DISCUSSION

As discussed before, the sample-based stochastic model provides output distribution with respect to uncertain input distribution and how uncertain input parameters affect these output parameters will be discussed in this section. If true distribution of the output is required, large numbers of input samples are needed. Due to the massive computation and inefficiency caused by increasing input sample quantity, a minimum number of input parameters N which can represent input sample distribution as well as guarantee steady output distribution should be analyzed.

In the process to obtain N, we assume the nominal mean value of J, r_0, t_p, T_i are $1.2\mathrm{J/cm^2}$, $11 \times 10^{-6}m$, $50 \times 10^{-9}m$, 800K and the COV of each input parameter are set to be 0.02. Figure 3 presents the stochastic convergence analysis of the mean value of input parameters J, r_0, t_p, T_i. When the number of samples is less than 200, mean values of input parameter fluctuate frequently. At N = 200, the mean values of input parameters still oscillate but the amplitude is bounded within a small range which is less than 1%. In other words, 200 samples are enough to make sure nominal mean values of input parameters are steady.

Figure 4 presents the stochastic convergence analysis of the standard deviation of input parameters J, r_0, t_p, T_i. It is seen from Fig. 4 that although mean value of input parameters converge quickly and 200 samples are enough to guarantee steady nominal mean value, standard deviation still oscillates largely with more than 300 input samples. The reason for this is that deviation is a higher order moment and converges much slower than the mean value [12]. When sample number increases to 400, standard deviation of J, r_0, t_p, T_i converges within 6%, 8%, 2.5%, 2%, respectively.

Similarly, after applying stochastic convergence analysis to output mean value, Fig. 5 can be obtained. Similar to with the mean value of input parameters, output parameters mean value converges very fast. When the number of samples increases beyond 300, mean values of all output parameters will be within 1%.

Presented in Fig. 6 is stochastic convergence analysis of standard deviation of output parameters. Standard deviation converges within 9% for T_{surf}, 16% for S_s, 11% for S_{lvm}, 9% for T_{sat}, 9% for P_{sat}, 10% for t_{Ss} when 300 samples areexamined while within 3% for all output parameters when 400 parameters are used.

Thus, the minimum number of samples of N=400 is obtained and this number of samples will be used to conduct following analysis. Figure 7 gives a typical distribution of output parameters when nominal mean value of J, r_0, t_p, T_i are $1.2\mathrm{J/cm^2}$, $11 \times 10^{-6}m$, $50 \times 10^{-9}m$, 800K and the COV of each input parameter are 0.02. The histograms of T_{surf}, S_s, S_{lvm}, T_{sat}, P_{sat} and t_{Ss} corresponding to stochastic model with 400 samples are presented. In the histograms, distribution of output parameters is no longer Gaussian distribution. This is due to highly nonlinear effect in the solid-liquid-vapor phase change process. P5, P25, P50, P75, P95 in Fig. 8 refer to 5th, 25th, 50th, 75th, and 95th percentiles in the histograms respectively. IQR as defined previously is interquartile range which is the difference between P75 and P25. It can be easily concluded from the histograms that the variability of output parameters will decreases as IQR decreases. This is why IQR can be used to quantify the uncertainty of output parameters.

Presented in Fig. 8 are IQR of T_{surf}, S_s, S_{lvm}, T_{sat}, P_{sat} and t_{Ss} as a function of COV of input parameters J, r_0, t_p, T_i. It should be emphasized that when COV of one input parameters increases from 0.01 to 0.03, COV of other parameters are kept constant at 0.01.

In IQR analysis of maximum surface temperature T_{surf}, IQR of T_{surf} increases significantly from 43.56K to 77.07K when COV of J increases from 0.01 to 0.03. This result indicates that surface temperature of metal powder particle deeply depends on energy of laser, which is a well recognized fact. On the other hand, COV of radius and initial temperature of metal powder particles is relatively less important to the surface temperature.

In IQR analysis of maximum solid-liquid interface S_s, laser fuence J is also influential to the IQR of S_s. Besides, when initial temperature of metal particles Ti increase from 0.01 to 0.03, IQR of Ss also gives an observable increase, i.e., from 0.01452 μm to 0.01921 μm. A convincing explanation is that metal particle with lower initial temperature absorbs more energy to reach melting point. IQR analysis of S_{lvm}, T_{sat}, P_{sat}, t_{Ss} all indicate a strong relationship between IQR and COV of J while variability of other input parameters have little influence on IQR.

Figure 8 indicates a strong relationship between IQR and COV of J so relationship between IQR of output parameters and different value of J is also worth investigating. Figure 9 presents IQR of T_{surf}, S_s, S_{lvm}, T_{sat}, P_{sat} and t_{Ss} at different laser fluence and different COV of J. As noted above, when COV of J increases from 0.01 to 0.03, COV of other parameters stay constant. It can be observed from Fig. 9 that: (1) at different laser fluence, COV of J still significantly causes increasing of IQR of output parameters; and (2) as laser influence increases from $1.0 \times 10^4\mathrm{J/m^2}$ to $1.2 \times 10^4\mathrm{J/m^2}$ and then to $1.4 \times 10^4\mathrm{J/m^2}$, IQR of T_{surf}, S_s, S_{lvm}, T_{sat}, P_{sat} and t_{Ss} increase. It indicates high dependence of T_{surf}, S_s, S_{lvm}, T_{sat}, P_{sat} and t_{Ss} on the laser fluence.

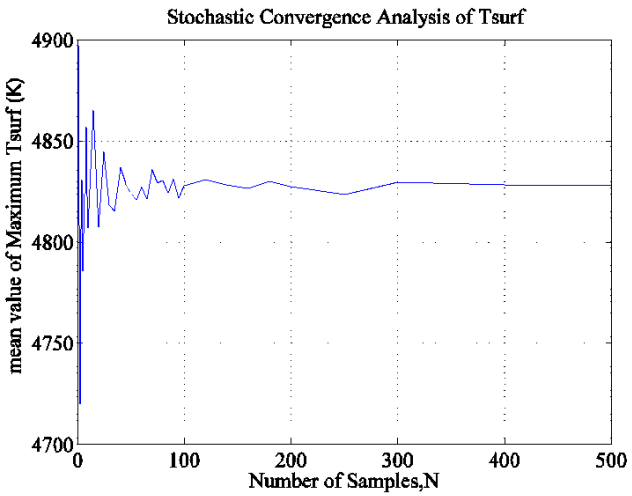

(a) Convergence Analysis of Mean Value of T_{surf}

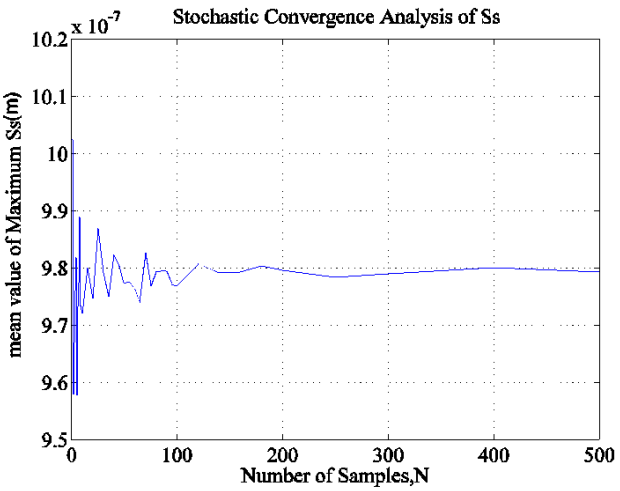

(b) Convergence Analysis of Mean Value of S_s

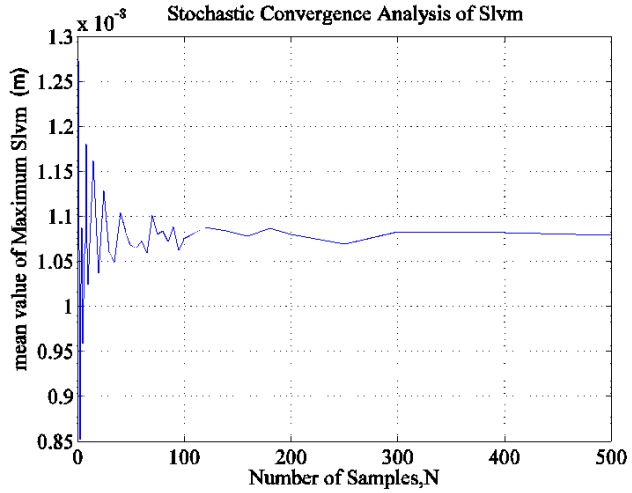

(c) Convergence Analysis of Mean Value of S_{lvm}

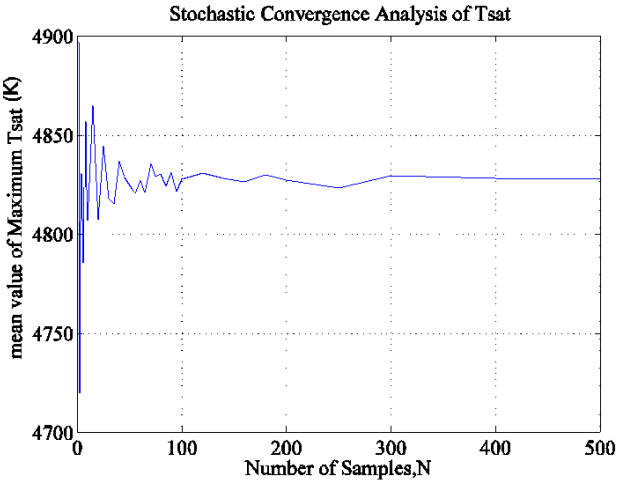

(d) Convergence Analysis of Mean Value of T_{sat}

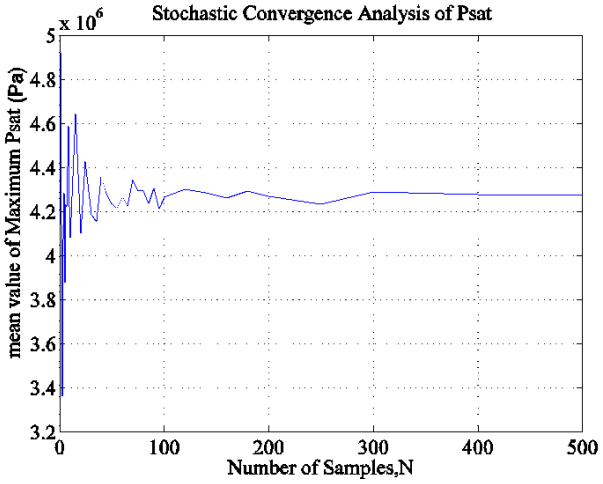

(d) Convergence Analysis of Mean Value of P_{sat}

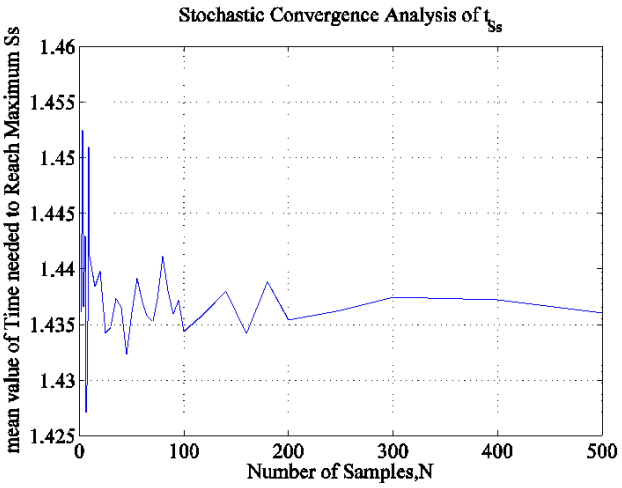

(d) Convergence Analysis of Mean Value of t_{Ss}

Fig. 5 Stochastic Convergence Analysis of Mean Value of Output Parameters

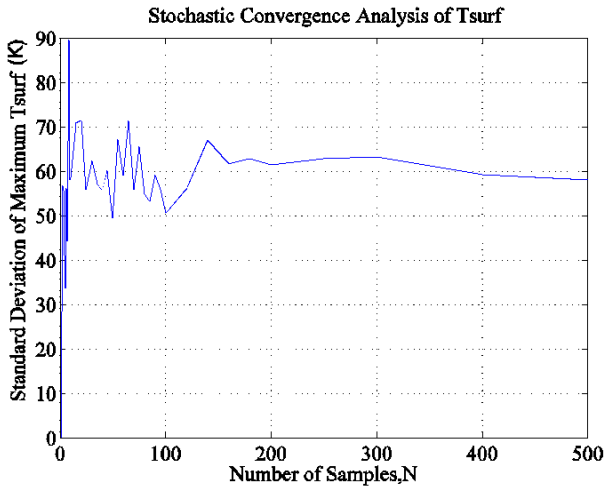

(a) Convergence Analysis of Standard Deviation of T_{surf}

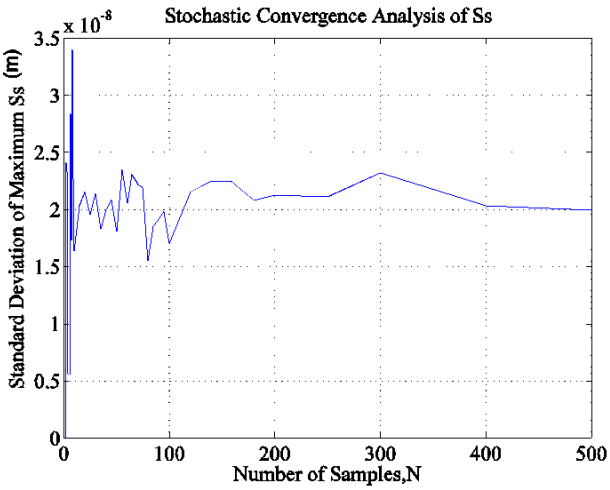

(b) Convergence Analysis of Standard Deviation of S_s

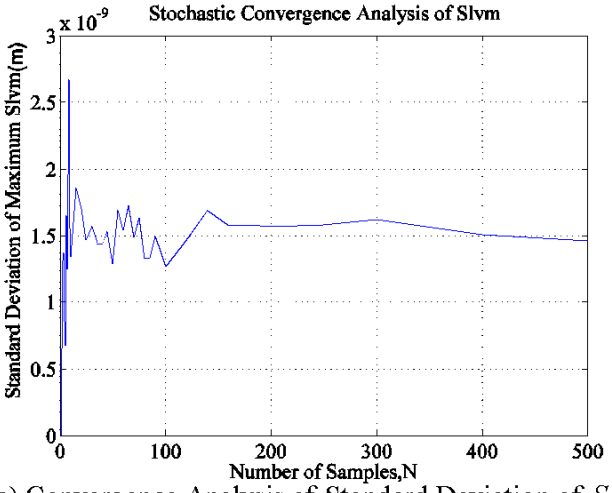

(c) Convergence Analysis of Standard Deviation of S_{lvm}

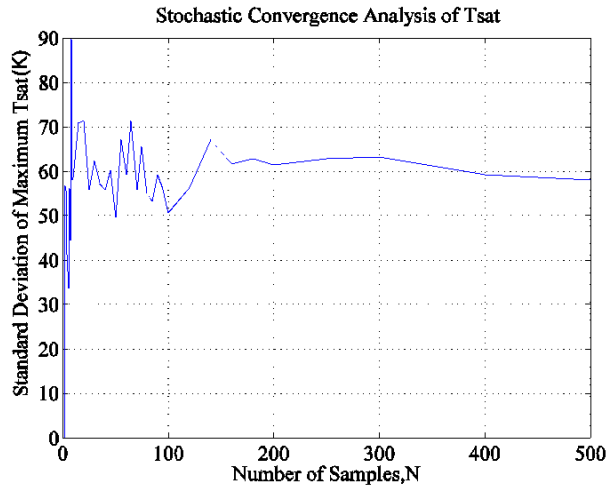

(d) Convergence Analysis of Standard Deviation of T_{sat}

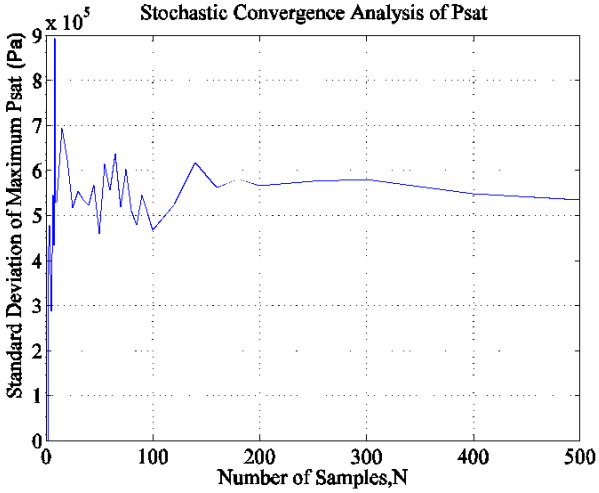

(e) Convergence Analysis of Standard Deviation of P_{sat}

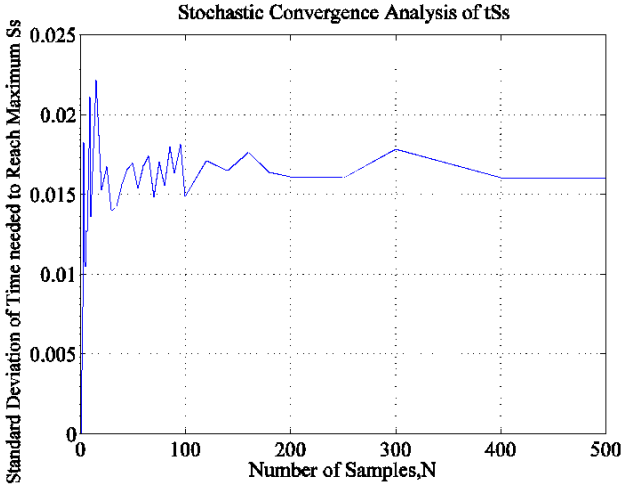

(f) Convergence Analysis of Standard Deviation of t_{Ss}

Fig. 6 Stochastic Convergence Analysis of Standard Deviation of Output Parameters

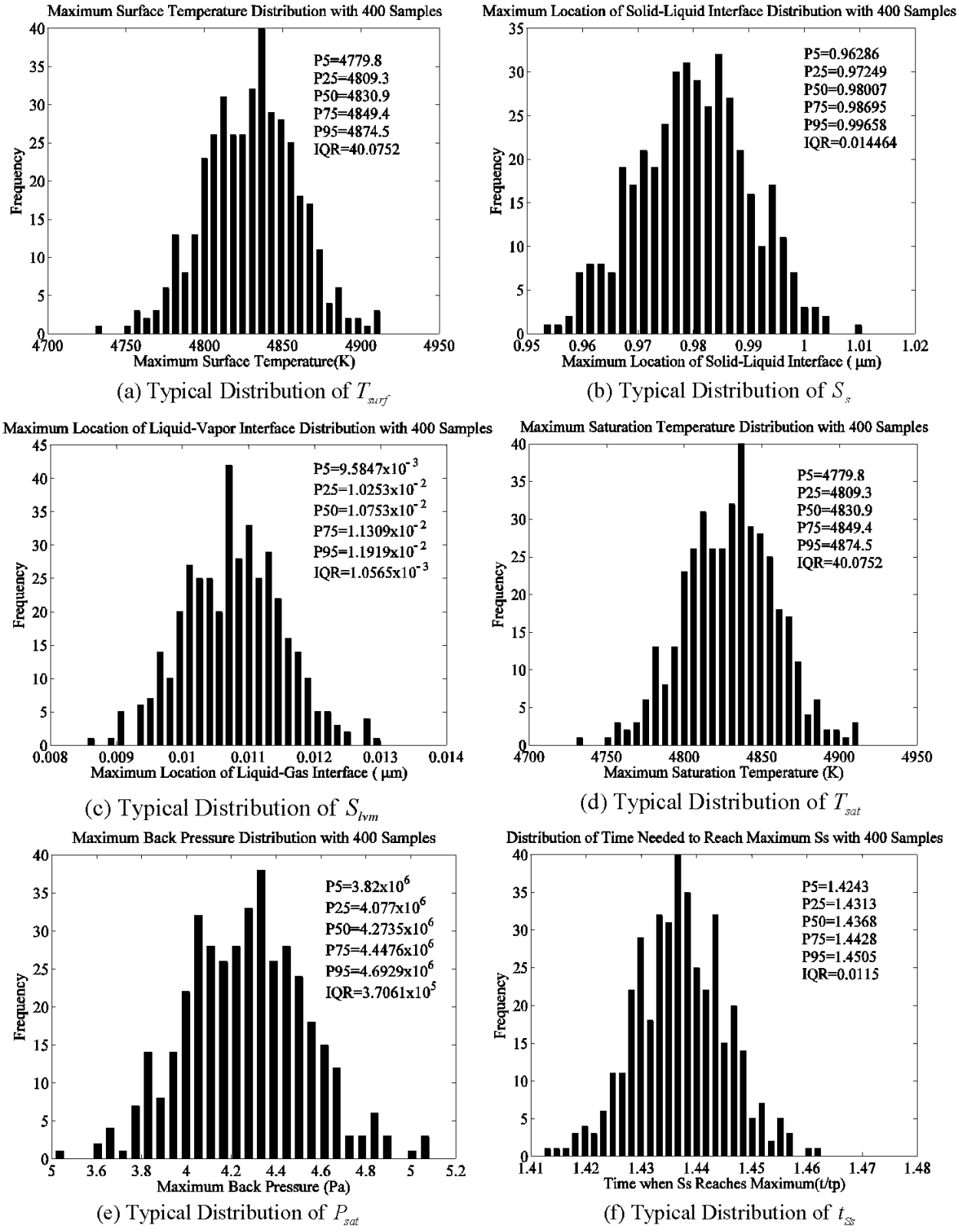

Fig. 7 Typical Distribution of Output Parameters

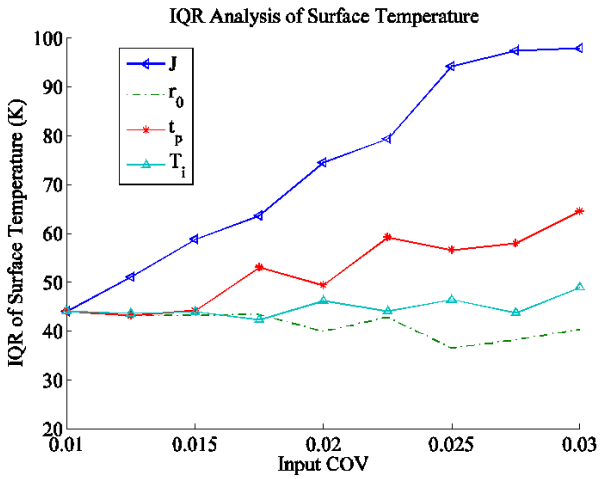

(a) IQR of T_{surf} with Different Input Parameters COV

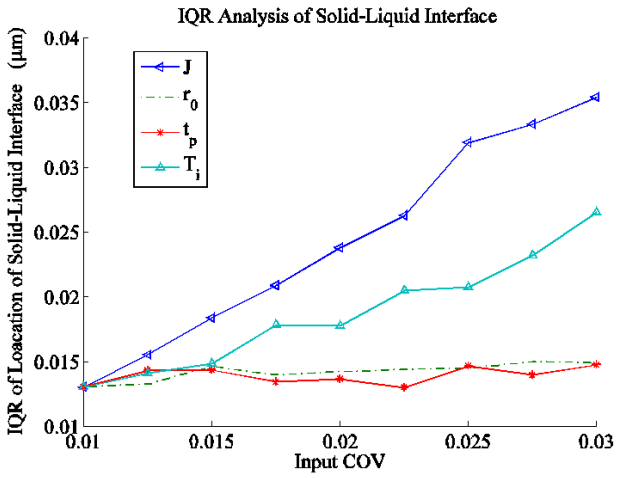

(b) IQR of S_s with Different Input Parameters COV

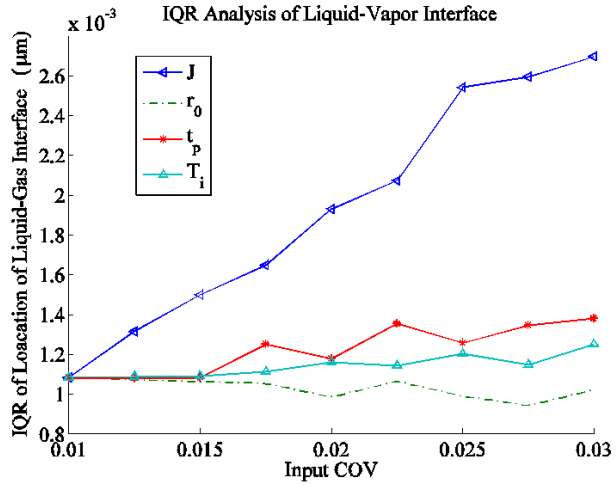

(c) IQR of S_{lvm} with Different Input Parameters COV

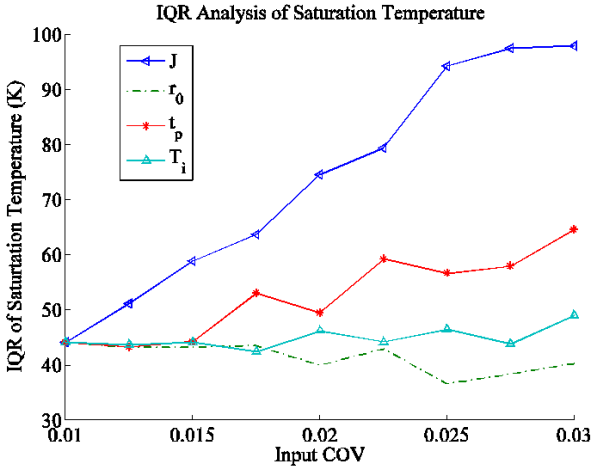

(d) IQR of T_{sat} with Different Input Parameters COV

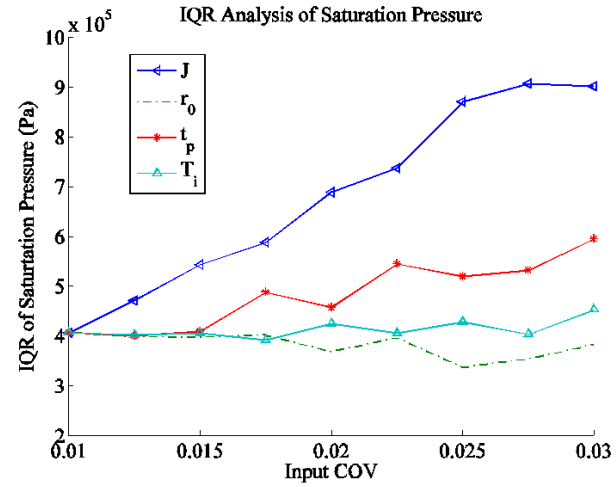

(e) IQR of P_{sat} with Different Input Parameters COV

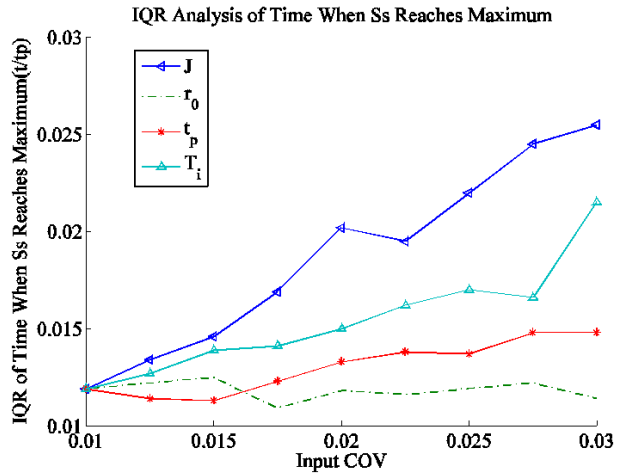

(f) IQR of t_{Ss} with Different Input Parameters COV

Fig. 8 IQR of Output Parameters with Different COV of Input Parameters

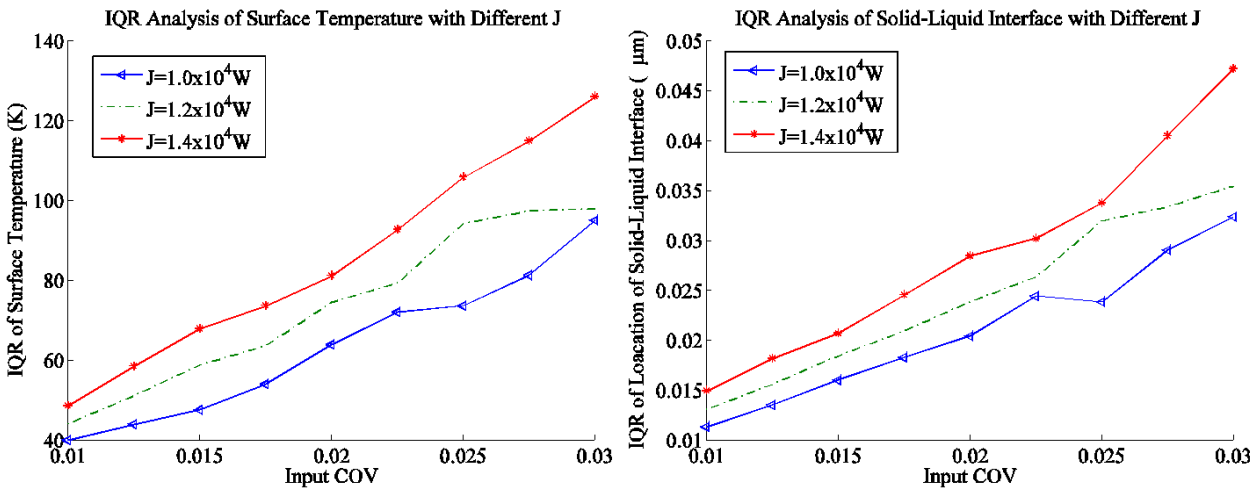

(a) IQR of T_{surf} with Different Value and COV of J (b) IQR of S_s with Different Value and COV of J

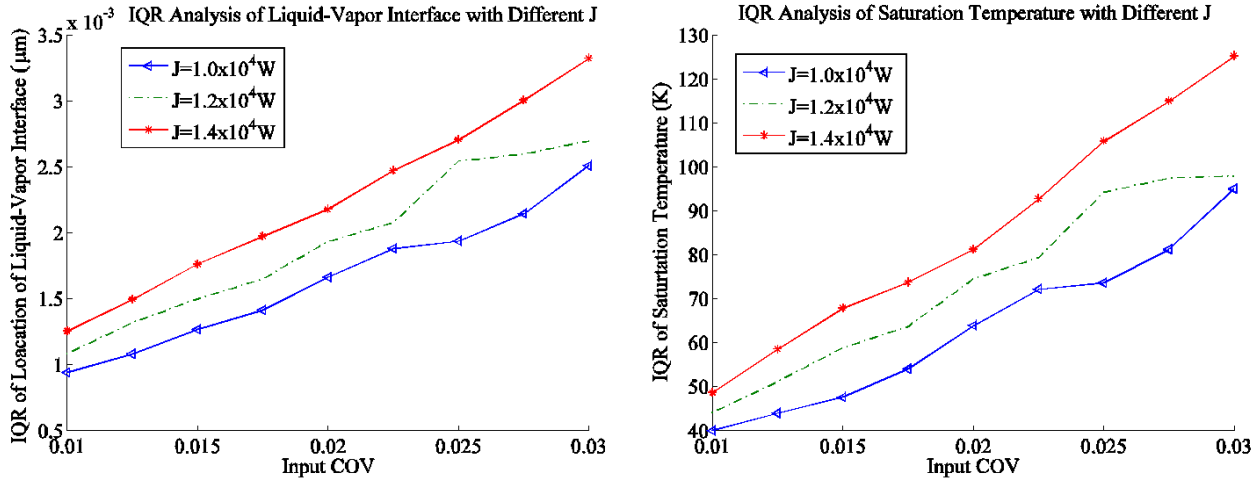

(c) IQR of S_{lvm} with Different Value and COV of J (d) IQR of T_{sat} with Different Value and COV of J

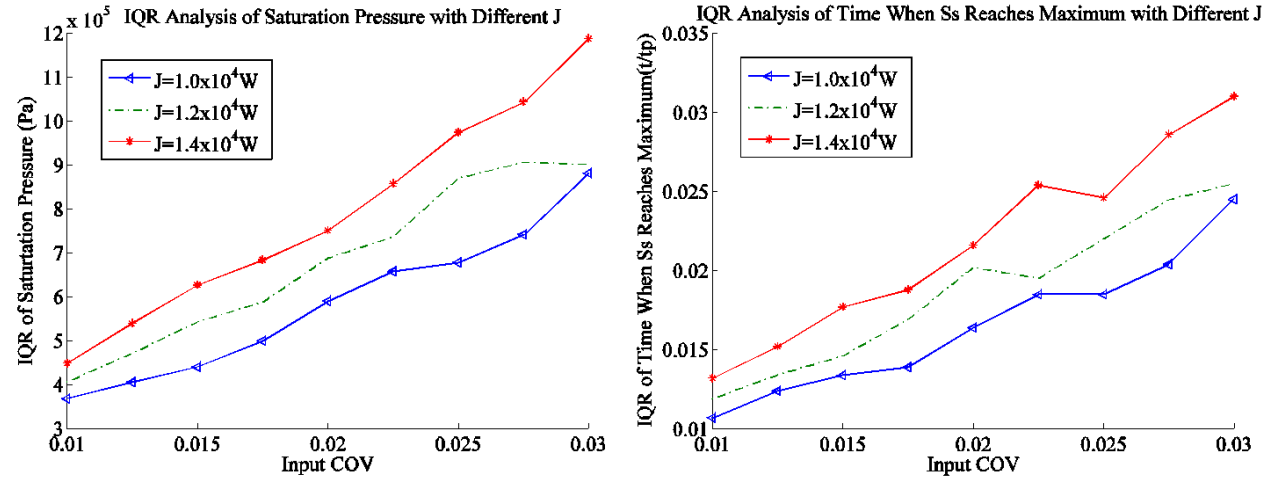

(e) IQR of P_{sat} with Different Value and COV of J (f) IQR of t_{Ss} with Different Value and COV of J

Figure 9 IQR of Output Parameters with Different Value and COV of J

CONCLUSIONS

Based on physical model of metal powder particle phase change, a stochastic model was presented to study the effects of uncertainty of input parameters on the results. COV is used to characterize variability of the input parameters and IQR is used to measure uncertainty of the output parameters. The IQR analysis shows that laser fluence has a dominant influence on metal powder article surface temperature, solid-liquid interface, liquid-vapor interface, saturation temperatures, saturation pressure and time needed to reach maximum solid-liquid interface, which serves guidance in SLS manufacturing process. Methods of analyzing uncertain output parameters with respect to uncertain input parameters can be generally applied to study other areas of engineering problem where input parameters vary.

ACKNOWLEDGEMENT

Support for this work by the U.S. National Science Foundation under grant number CBET- 1066917 is gratefully acknowledged.

REFERENCES

[1] Deckard, C.R., 1988, "Selective Laser Sintering," Ph.D. thesis, University of Texas, Austin, TX.

[2] Deckard, C.R., 1989, "Method and Apparatus for Producing Parts by Selective Sintering," US Patent No. 4, 538.

[3] Deckard, C.R., and Beaman, J.J., 1987, "Solid Freeform Fabrication and Selective Powder Sintering", Proc. 15th NAMRC-SME, Bethlehem, PA, pp. 636-640.

[4] Kumar, S., 2010, "Selective Laser Sintering: Recent Advances", 4th Pacific International Conference on Applications of Lasers and Optics, Wuhan, China, pp. 8.

[5] Bunnell, D.E., 1995, "Fundamentals of Selective Laser Sintering of Metals," Ph.D. thesis, University of Texas: Austin, TX.

[6] Fischer, P., Leber, H, Romano, V., Weber, H. P., Karapatis, N.P., Andre, C., and Glardon, R, 2004, "Microstructure of near-infrared pulsed laser sintered titanium samples," Applied Physics A: Materials Science and Processing, 78(8), pp. 1219-1227.

[7] Fischer, P., Romano, V., Blatter, A., and Webler, H. P., 2005, "Highly precise pulsed selective laser sintering of metallic powders," Laser Physics Letters, 2(1), pp. 48-55.

[8] Shi, Y., Zhang, Y., and Konrad, C., 2007, "Solid-Liquid-Vapor Phase Change of A Subcooled Metal Powder Particle Subjected to Nanosecond Laser Heating," Nanoscale and Microscale Thermophysical Engineering, vol. 11, pp. 301-318.

[9] Acquah C., Datskov, I., Mawardi A., Zhang F., Achenie L. E. K., Pitchumani R., and Santos E., "Optimization of an optical fiber drawing process under uncertainty," Indust. Eng. Chemistry Res., vol. 45, pp. 8475-8483, 2006.

[10] Padmanabhan S. K. and Pitchumani R., "Stochastic modeling of nonisothermal flow during resin transfer molding processes," Int. J. Heat Mass Transfer, vol. 42, No. 16, pp. 3057-3070, 1999.

[11] Diwekar, U. M. and Rubin, E. S., "Stochastic modeling of chemical process," Computer and Chemical Engineering vol.15, No. 2, pp. 105-114.

[12] Mawardi, A., and Pitchumani, R., 2008, "Numerical Simulation of an Optical Fiber Drawing Process Under Uncertainty," *Journal of Lightwave Technology*, vol. 26, No. 5.

[13] Myers M. R., "A model for unsteady analysis of preform drawing," AIChE J., vol. 35, No. 4, pp. 592-602, 1989.

[14] Campbell J. E. and Rao B. S. R., "An uncertainty analysis methodology applied to sheetpile Cofferdam design," Hydraulic Engineering, vol. 41, pp. 36–41, 1987.

[15] Apostolakis G., "The concept of probability in safety assessments of technological systems," Science, vol. 250, pp. 1359-1364, 1990.

[16] Mawardi A. and Pitchumani R., "Effect of parameter uncertainty on the performance variability of proton exchange membrane (PEM) fuel cells," J. Power Sources, vol. 160, pp. 232-245, 2006.

[17] Mawardi, A., and Pitchumani, R., 2004, "Cure Cycle Design for Thermosetting-Matrix Composites Fabrication under Uncertainty," *Annals of Operation Research*, vol. 132, pp. 19-45.

[18] Konrad, C., Zhang, Y., and Shi, Y., 2007, "Melting and Resolidification of Subcooled Metal Powder Particle Subjected to Nanosecond Laser Heating," International Journal of Heat and Mass Transfer, 50(11-12), pp. 2236-2245.

[19] Fisher, P., Romano, V., Weber, H.P., and Kolossov, S., "Pulsed Laser Sintering of Metallic Powders", Thin Solid Films, vol. 453-454, pp. 139-144, 2004.

[20] Bellantone R. and Ganesh R. K., "Analysis Model for Laser Hold Drilling", Final Report, Contract Ⅱ, Report submitted to Pratt and Whitney Aircraft, East Hartford, CT, 1991.

[21] Ganesh R. K., Faghri A., and Hahn Y., "A Generalized Thermal Modeling for Laser Drilling Process- I Mathematical Modeling and Numerical Methodology," International Journal of Heat and Mass Transfer, vol. 40, pp. 3351-3360, 1997

